Quantification and kinetics of nitrogen mass gain during high temperature oxidation of titanium in air

Victor Pacorel, Pascal Berger, Virginie Moutarlier, M. C. Marco de Lucas, Tony Montesin, Nicolas Geoffroy, Frédéric Herbst, Olivier Heintz, Virgil Optasanu, Luc Lavisse

Quantification and kinetics of nitrogen mass gain during high temperature oxidation of titanium in air

Victor Pacorel[1], Pascal Berger[2], Virginie Moutarlier[3], María del Carmen Marco de Lucas[1], Tony Montesin[1], Nicolas Geoffroy[1], Frédéric Herbst[1], Olivier Heintz[1], Virgil Optasanu[1], Luc Lavisse[1,*]

[1]Laboratoire Interdisciplinaire Carnot de Bourgogne (ICB), UMR 6303 CNRS-Université de Bourgogne, 9 Avenue A. Savary, BP 47 870, F-21078, Dijon, France

[2] Université Paris-Saclay, CEA, CNRS, NIMBE, 91191, Gif-sur-Yvette, France

[3] Institut UTINAM, UMR CNRS 6213, 16 Route de Gray, Université Franche-Comté, 25030, Besançon, France

Abstract (100 words)

Improving the high-temperature oxidation resistance of titanium alloys in air is a prerequisite for extending their use in turbojet engines. A better understanding of the role of atmospheric nitrogen is required for this purpose. Here, we studied the insertion kinetics of nitrogen in titanium at 650 °C in air up to 100 h. Moreover, the nitrogen mass gain, and its ratio over the total mass gain, were quantified as a function of the oxidation duration by using Nuclear Reaction Analysis. It was found that nitrogen inserts into titanium with a parabolic kinetics and a rate constant about 1500 times smaller than oxygen.

Keywords: High-temperature oxidation; titanium; nitrogen insertion kinetics; nuclear reaction analysis; glow discharge optical emission spectrometry

1. Introduction

Titanium alloys are of great interest to the aerospace industry as a replacement for higher-density alloys, with the aim of reducing aircraft weight and hence operating costs. They are currently used, for example, in turbojet engines, for fan and compressor parts, where temperatures can reach a maximum of about 600 °C [1], [2], [3]. Above this temperature, the rapid oxidation of titanium alloys makes them unacceptable for the hottest parts of turbo engines. These parts require materials with a higher oxidation resistance, such as superalloys based on nickel, cobalt, or iron-nickel systems [4], which have a higher density than titanium. High-temperature oxidation of titanium leads not only to the formation of an oxide layer on the surface, but also to the dissolution of oxygen in the underlying metal, which has a major impact on the mechanical properties [5]. The development of titanium alloys for aerospace applications is aimed at increasing the service temperature, as well as guaranteeing the thermal stability of the alloys and their mechanical properties, particularly resistance to creep at high temperatures [6], [7].

In the last 30 years, several papers have shown a link between the insertion of nitrogen during oxidation and a better oxidation resistance of titanium alloys at high temperature [8], [9], [10], [11], [12], [13], [14], [15], [16]. In 1986, Chaze and Coddet [8] reported for the first time the reduction in the oxidation rate of titanium and its alloys, when oxidized in air, compared with an oxidation under pure oxygen, for temperatures ranging from 550 to 700 °C. This highlighted the important role of nitrogen in high-temperature oxidation in air. Inserted nitrogen tends to accumulate at the oxide-metal interface, which can be explained by a higher diffusion coefficient of nitrogen than oxygen in the rutile phase of titanium dioxide [17], not yet clearly determined, whereas the diffusion coefficient of nitrogen is ten times lower than that of oxygen in titanium [18], [19], [20].

More recently, Kanjer et al. [10] managed to characterize more accurately than Chaze and Coddet the oxide-metal interface in commercially pure titanium oxidized for 100 h at 700 °C in dry air. Using Nuclear Reaction Analysis (NRA), the formation of a discontinuous nitrogen-rich layer at the oxide-metal interface was shown. More interesting, the same material being treated by laser shock peening prior to the oxidation, presented a continuous nitrogen-rich layer, as well as a thinner, more compact, and more adherent oxide scale and thinner α-case zone than the untreated material. This observation shows that the presence of this continuous nitrogen-rich zone is associated with an improved oxidation resistance. Kanjer et al. [10] also suggested that the enhanced adherence of the oxide in the presence of this continuous nitrogen-rich zone could be explained by the presence of oxynitrides layers located between the oxide and the nitrogen rich-zone. Indeed, such a layer could allow the Pilling-Bedworth ratio (1.76 for Ti/TiO_2, [21]) to evolve smoothly from the oxide to the metal. This hypothesis, concerning oxynitrides layers, was verified by Abdallah et al. [13] on Ti6242S alloy oxidized in synthetic air at 650 °C for 1000 hours. Using Electron Energy Loss Spectroscopy (EELS), they demonstrated a gradient in nitrogen concentration which reaches a maximum at the oxide-metal interface, and gradually decreases when moving away from this zone, towards the surface or the bulk of the material. They reported the formation, beneath the TiO_2 rutile layer, of a 13 nm-thick TiO_xN_y (FCC) oxynitride layer, a 30 nm-thick nitride zone composed of TiN (FCC) and Ti_2N, and finally N-rich α-Ti. The same alloy, oxidized in an N_2-free atmosphere (80% Ar - 20% O_2), showed an oxide layer five times thicker than that oxidized in air.

The formation of an interfacial layer of Ti_2N phase under the oxide was also shown by Lavisse and al. [16] for commercially pure titanium oxidized at 700 °C for 5 h in air, as well as for shot-peened and laser-shock treated titanium. However, only laser-shock treated titanium showed the formation of a continuous nitrogen rich zone. The protective role of this layer in slowing

down the diffusion of oxygen into the metal was confirmed by the in-depth micro-hardness profile along the cross-section.

Aldaz Cervantes [22] has investigated the oxidation of pure and commercially-pure Ti for short durations at 800 °C under low pressure of different mixtures of oxygen and nitrogen in argon in order to investigate the influence of nitrogen. As a function of the gas environment, it was found the formation in the scales of ε-Ti_2N, TiN, fcc rocksalt Ti oxynitrides, Ti_2O_3 corundum and Magnéli phases in addition of rutile. In particular, an interfacial N-rich layer was found in pure titanium at the early stages of oxidation under ultra-high purity Ar (N_2:O_2 = 5).

Göbel et al. [23] used isotopic tracers to study the oxidation of pure titanium at 800 °C in dry and humid air and used secondary neutral mass spectrometry (SNMS) to study the depth-dependent distribution of nitrogen and oxygen in oxide scales. They showed the formation of a nitride layer at the interface between the scale and the metal, but the mass gain corresponding to nitrogen could not be determined by SNMS.

Recently, Optasanu et al. [15] used isotopic labelling to track nitrogen diffusion during titanium oxidation in air at 700 °C and reported the first measurements of nitrogen mass gain using nuclear reaction analysis. Their results showed that nitrogen accounted for 16% of total mass gain in samples oxidized for 5 hours, but only 12.5% in samples oxidized for 20 hours, even though nitrogen mass gain almost doubled between 5 and 20 hours of exposure.

While the insertion of nitrogen during the high temperature oxidation of titanium in air, and its tendency to slow down the oxidation rate, is attested by previous works, the mechanisms of insertion and the limiting-step in this process have not yet been elucidated. To our knowledge, no study has been published to date on the kinetics of nitrogen insertion during the oxidation process, which is a fundamental point to investigate the mechanism. Knowledge of these

kinetics could bring us closer to control this process, and thus indirectly to influence overall oxidation kinetics. In addition, several studies have suggested a synergistic effect between certain alloying elements, such as niobium or silicon [24], [25], and nitrogen on resistance to high-temperature oxidation. Knowing the kinetics of nitrogen insertion in pure titanium will be very useful in understanding the effect of different alloying elements and the influence of nitrogen. Finally, measuring the amount of nitrogen inserted can be useful for thermodynamic simulations of the stability of nitride phases.

The aim of this work is to fill this information gap on nitrogen insertion, so here we address the study of the kinetics of nitrogen mass gain in commercially pure titanium oxidized at 650°C in laboratory air from the early stages of oxidation up to 100 hours. Moreover, the goal is to quantify the nitrogen mass gain as a function of the oxidation duration and its ratio over the total mass gain. Two main techniques, Glow Discharge Optical Emission Spectrometry (GDOES) and Nuclear Reaction Analysis (NRA), have been used to study the distribution of nitrogen as a function of the depth in samples oxidized for durations up to 100 h. Nitrogen quantification was carried out using NRA, which is particularly a well-suited technique for this end. Unlike other techniques already used to detect the presence of nitride phases in oxidized titanium alloys, such as atom probe tomography [24], [25], [26] or transmission electron microscopy [13], NRA is depth-resolved, so characterizations can be carried out from the surface, without any specific preparation. The detected signal is proportional to the quantity of nitrogen atoms in the sample, enabling absolute measurement. Other advantages of NRA are the absence of matrix effects and the ability to easily differentiate between nitrogen and titanium signals, which can be difficult with other techniques such as EDS/WDS analysis. Grazing incidence X-ray diffraction analysis and cross-sectional SEM/EDS/WDS observations of oxidized samples were used to study the crystalline phases formed and the depth localization of nitrogen, respectively.

2. Materials & Methods

2.1 Sample preparation

The material used in this study was a 2 mm thick plate of commercially pure titanium, (grade I, certified purity 99.6%, Goodfellow). Two sets of eleven samples each were prepared from this plate: small pieces measuring 20 × 10 × 2 mm^3 (for NRA and SEM analysis) and larger pieces measuring 20 × 15 × 2 mm^3 (for GDOES analysis, which requires samples larger than 10 mm, and for XRD analysis). Cutting was carried out using a SiC GC 150NB34 disc on a PRESI Mecatome T201A automatic micro-cutting machine. The resulting parts were then hand polished up to P1200 grit SiC abrasive paper and cleaned with ethanol in an ultrasonic bath for 2 minutes.

For SEM cross-section observation, the oxidized samples were cut using a micro-cutting machine, then prepared as follows: 1- gold-plated by EDWARDS ScanCoat Six sputtering, copper-plated by electrodeposition, 2- conductive resin-coated with PRESI Mecapress 3, 3- automatically polished with SiC abrasive papers to P1200 grit, 4- mirror-polished (superfinished with 30 nm silica colloidal suspension) and 5- cleaned with ethanol in ultrasonic bath.

2.2 Oxidation tests

Samples were weighed on Mettler Toledo AB135-S/FACT balance with 0.07 mg accuracy and their dimensions were measured with a digital calliper IHM 1150 MI with 10 µm accuracy.

The two series of eleven samples were isothermally oxidized in a Magma Therm muffle furnace at 650 °C in laboratory air. High-temperature exposure durations ranged from 15 minutes to 100 hours. One small and one large sample were taken from the furnace for each exposure

duration. After measuring their mass, they were studied from the surface by GDOES, NRA and XRD.

2.3 Analysis techniques

Scanning Electron Microscope JEOL JSM-7600F was used to study the cross-section of the sample oxidized 16 h. Back-scattering electron (BSE) analysis was used to observe the oxide/metal interface. An energy dispersive spectrometer (EDS, Oxford instruments SDD X-MAX 80 mm²) was used to map the distribution of titanium and oxygen on cross-sections, while a wavelength dispersive spectrometer (WDS, Oxford instruments INCA WAVE 700) was used to map the distribution of nitrogen.

X-ray diffraction was used to identify the crystalline phases present in the samples. Diffraction patterns recorded in grazing incidence ($\theta_{inc} = 8°$) were obtained with a Bruker D8-A25 Discover goniometer, equipped with a copper anticathode ($\lambda_{K\alpha 1\text{-}2} = 1.5419$ Å) and a LYNXEYES-XE detector. The detection range of 2θ was from 20 to 80° with a step size of 0.03° and an acquisition time of 6 s per step.

Glow-Discharge Optical Emission Spectroscopy was used to study the in-depth elemental composition. The spectrometer was a Jobin-Yvon Horiba GD Profiler (U = 600V), calibrated on aluminium ray with a pure aluminium plate. The size of the zone analysed was 4 mm in diameter. The distribution of oxygen, nitrogen and titanium was monitored by measuring over sputtering time the evolution of the intensity of the characteristic radiation for each element: 130.21 nm, 149.26 nm and 365.35 nm respectively.

Quantification of nitrogen in oxidized samples was studied by Nuclear Reaction Analysis [27], [28] at CEA Saclay (NIMBE-LEEL Laboratory of CNRS/CEA), France [29], [30]. This technique is well suited to the detection and quantification of elements, particularly light elements such as oxygen and nitrogen, with a sensitivity of around 0.1 at.% and an accuracy around 1% [31]. A deuteron (d+, deuterium ion) microbeam was directed perpendicularly to the samples surface. The energy of the beam was fixed at 1.9 MeV, the highest deliverable by the accelerator for deuteron beams, to maximize the cross-section of the nuclear reactions on ^{14}N isotope. At this energy, other light elements such as ^{16}O and ^{12}C also produce nuclear reactions in these conditions.

Among the various nuclear reactions of the ^{14}N isotope, the chosen one to quantify nitrogen concentration is the reaction $^{14}N(d,\alpha_1)^{12}C$ [16], [15]. This formalism expresses that a high-energy deuteron (d) reacts with a ^{14}N nucleus to produce a ^{12}C nucleus at its first excitation state (1) and an alpha particle (α). The detection of backscattered deuterons and particles produced by the nuclear reactions was set at 170° from the incident deuteron beam using an annular surface barrier detector.

For 1.9 MeV incident deuterons, the calculated energy released by the nuclear reaction $^{14}N(d,\alpha_1)^{12}C$ is equal to 9136 keV, and the produced alpha-particle has an energy of 6788 keV when the reaction takes place at the sample surface. If the reaction takes place under the surface of the material, both the incident deuteron beam and the emitted alpha particle lose energy. The PYROLE software [32] can be used to calculate the energy loss of particles through the material being analysed as a function of incident beam conditions and the nature of the sample. Then, the energy shift of the detected alpha particles can be used to determine the in-depth localization of nitrogen. The intensity of the signal (number of the detected events) is proportional to the concentration of nitrogen atoms inserted in the material weighted by the probability (cross-

section) of the reaction to occur. The oxide formed above the nitrogen-rich layer is mainly TiO_2, in rutile form, with a known stopping power. We can therefore deduce the depth distribution of the nitrogen [16], [15]. Although NRA spectra can be directly simulated with the help of dedicated codes, we have chosen to determine the nitrogen quantity by comparison with a TiN standard. The concentration profile of nitrogen can be extracted from NRA spectra from the surface over depths of several micrometres, without any destructive preparation [15].

3. Results and discussion

3.1 Kinetics of the oxidation process over 100 h

Figure 1 shows the variation of the mass gain as a function of square root of time for CP-Ti samples oxidized in air at 650 °C for 100 h. The results obtained for the two series of samples (i.e. small and large samples) are similar. The classic Wagner theory of oxidation [21] shows that for a diffusion driven oxidation process the mass gain follows a parabolic evolution :

$$\frac{\Delta m}{S} = {k_p}^{1/2}.t^{1/2} \qquad (1)$$

where Δm is the mass variation, S the sample surface, t the time and k_p the parabolic rate constant. The Fig. 1 shows a linear evolution of the mass gain with respect to the quare root of time (R^2 close to 1 for each series of samples), which corresponds to the equation (1). The calculated k_p value is 53×10^{-4} mg^2 cm^{-4} h^{-1}. This value is consistent with the value of 120×10^{-4} mg^2 cm^{-4} h^{-1} reported by Chaze and Coddet [8] for T35 alloy after 40 h of oxidation at 650 °C in air. The parabolic kinetics is characteristic of the formation of a dense, protective oxide layer, and suggest a mechanism based on diffusion through the growing oxide layer.

3.2 Structure and phases of the oxidized samples

The XRD patterns obtained with fixed incident angle of 8° before and after oxidation for 16 and 80 h at 650 °C are presented in Figure 2. The patterns of the oxidized samples show mainly diffraction peaks assigned to the rutile phase of TiO_2 and to α-Ti(O,N), which is a solid solution of oxygen into α-Ti with a possible minor contribution of nitrogen. The relative intensity of rutile peaks increases between 16 and 80 h of exposure, suggesting that the oxide layer (mainly composed of rutile TiO_2) grows with the high temperature exposure duration.

After 80 h of oxidation, new peaks can also be distinguished in the XRD pattern (Fig. 2 and S1) at around 39.2°, 42.6° and 69.0°. Two of these, at 39.2° and 69.0°, could correspond to XRD peaks reported for tetragonal titanium nitride $Ti_2N_{0.84}$ (ICDD 04-002-0574), while the very weak peak at 42.6° could correspond to a XRD peak of titanium oxynitride $TiN_{0.67}O_{0.23}$ (ICDD 04-006-2333). However, the intensity of these peaks is very low, and the proximity of peaks of the main phases (TiO_2 and α-Ti(O,N)) makes difficult their clear assignment. The quantity and size of nitride grains remain uncertain, but the formation of titanium nitrides has already been reported by Optasanu et al. [15] for CP-Ti oxidized at 700 °C for short oxidation durations (20 hours), and by Lavisse et al. [16] for shot-peened and laser-shock peened CP-Ti oxidized at 700 °C for 10 hours. Moreover, Abdallah et al. [13] and Dupressoire et al. [12], [14] reported the formation of nitrides and N-rich α-Ti zones in Ti6242S oxidized for 1000 h at 650 °C in air.

Figure 3.a, e, f, and g show a SEM cross-section image in BSE mode of a sample oxidized for 16 hours at 650 °C in air. The oxide scale (labelled “Ox” in Fig. 3.a) has an inhomogeneous thickness ranging from about 300 nm to 1.3 µm (Figs 3.f and 3.g). SEM observations at lower magnification are given as Supplementary Information (Fig. S2.a). They show alternating thin and thick zones in the oxide scale all along the cross-section of the sample. Between the oxide layer and the underlying metal, a dark grey zone is visible in Figure 3.a. Higher magnification

images (Figs. 3.f and 3.g) of thin and thick zones in the oxide scale, suggest the presence of porous oxide close to the oxide-metal interface. The formation of voids at the metal-oxide interface has been reported by Aldaz Cervantes [22] in CP-Ti oxidized at 800 °C for short durations (up to 25h) under low partial pressures of different mixtures of oxygen and nitrogen, but the mechanism of void formation has not been elucidated.

Figures 3.b, 3.c and 3.d show the spatial distribution of, respectively, oxygen (in light blue), nitrogen (in green) and titanium (in yellow) on the cross-section analysed by EDS for oxygen and titanium and by WDS for nitrogen. It is interesting to note that nitrogen is heterogeneously distributed, with the highest concentration beneath the oxide layer in areas where it is thinner, on the metal side, down to a depth of around 500 nm. This is in line with the results reported by Kanjer et al. using NRA [11] who showed the formation of a discontinuous nitrogen-rich layer at the oxide-metal interface in CP-Ti oxidized at 700 °C. In addition, a detailed observation (Fig. 3.e) of the oxide-metal interface in regions of higher nitrogen content reveals the presence of smaller grains, with sizes ranging from 20 to 100 nm. These observations are in agreement with those reported by Kitashima et al [33] who showed for the near-α titanium alloy TKT 41 oxidized at 750 °C the formation of recrystallized fine grains in the substrate near the oxide-metal interface. The concentration of nitrogen was higher in these recrystallized grains forming nitrogen-rich areas, while the concentration of oxygen was smaller in the recrystallized grains compared to the non-recrystallized grains. A similar result is observed here as there is less oxygen in nitrogen-rich zones than deeper in the titanium.

Under the nitrogen-rich zone (Fig. 3.c), the signal attributed to nitrogen in the WDS spectra recorded to map the sample cross-section is extremely weak. It does, however, appear slightly higher than in and above the oxide layer. This result needs to be treated with great caution, as the energy of the K_α X-ray line of nitrogen (0.392 eV) is so close to that of titanium (0.452 eV)

that it is extremely difficult to discriminate a very weak nitrogen signal when the titanium signal is so dominant.

3.3 Elemental composition profiles by GDOES

GDOES analysis was carried out on the surface of all samples. The size of the GDOES analysis zone was 4 mm in diameter, giving an average elemental composition over both thin and thick oxide layer zones observed by SEM.

Figure 4.a displays the evolution of the intensity of radiation characteristic of nitrogen (λ = 149 nm), oxygen (λ = 130 nm) and titanium (λ = 365 nm), as a function of the erosion duration for the sample oxidized for 15 minutes. This figure shows that nitrogen is detected, and so inserted into titanium, from the first stages of oxidation (15 minutes) with a location between an oxygen-rich zone and a titanium-rich zone which are likely to be respectively the oxide and the metal. This result agrees with the state of the art concerning the localization of nitrogen at the oxide/metal interface during titanium oxidation [8], [10], [11], [13], [15] as well as with our SEM observations.

The absolute GDOES signal intensity of different elements cannot be compared, but it is possible to compare the profile of a single element for different samples. Figure 4.b displays nitrogen profiles obtained for samples oxidized for 15 minutes, 2 h, 16 h, and 100 h. It shows that the longer the oxidation, the deeper the nitrogen is localized. The corresponding profiles obtained for titanium and oxygen over sputtering time are given as Supplementary Information (Figures S3 and S4). They show that nitrogen is localized at the metal/oxide interface for all high-temperature exposure durations studied here. At the oxide/metal interface, the oxygen signal decreases sharply, while the titanium signal increases sharply. The signal corresponding to nitrogen is observed at the intersection of the oxygen and titanium profiles, i.e. at the

metal/oxide interface. The sharpness of the variation in oxygen and titanium profiles at the interface in figures S3 and S4 decreases for longueur oxidation durations. This can be explained by the effect of a longer erosion time required for sputtering of a thicker oxidation layer. As the oxide layer thickens for longer exposure durations, the nitrogen is progressively localized deeper. This localization of nitrogen is consistent with the WDS mapping of nitrogen distribution (Fig. 3.c) in the sample oxidized 16 h which shows that the nitrogen is mainly localized at the oxide/metal interface in the metal side.

Figure 4.b also shows a broadening of nitrogen concentration profiles with increasing oxidation time. At first glance, this broadening suggestss an increasing presence of nitrogen in the oxidation layer forming an TiO_xN_y oxynitride, or in the form of a solid solution Ti(N), as observed by Abdallah et al. in Ti6242S oxidized for 1000 h at 650 °C under air [13]. The WDS mapping of the nitrogen distribution (Fig. 3.c) in a sample oxidized for 16 h does not allow us to assess the validity of this explanation. Moreover, the GDOES concentration profiles of titanium and oxygen (Figures S3 and S4) also show a broadening at the oxide-metal interface. The variations observed in the thickness of the oxide layer for 16 h of oxidation (Fig.3 and S2) may at least partly explain these effects, but we cannot neglect the effects due to sputtering over increasingly long durations. The depth-resolution of GDOES profiling has been investigated in several works which have shown a progressive loss of depth resolution due to the effects of sputtering as crater shape, roughness and preferential sputtering [34], [35], [36].

To study the kinetics of nitrogen insertion as a function of oxidation duration, the nitrogen profiles obtained by GDOES were integrated over the full duration of erosion. The values obtained, give a qualitative evolution of the quantity of nitrogen inserted. They are given in Figure 5 as a function of the square root of the oxidation time, $t^{1/2}$. It shows that nitrogen amount increases approximately linearly with $t^{1/2}$, despite a certain dispersion of values for shorter oxidations. This variation corresponds to a parabolic kinetics law for nitrogen insertion. A

similar analysis was carried out for oxygen insertion by integrating oxygen GDOES profiles. The results are given in Figure S5 as a function of the square root of the oxidation time. They also show roughly a linearly variation. This is in line with the variation in total mass gain (Fig. 1), which shows parabolic kinetics as a function of exposure time.

3.4 Quantifying nitrogen mass gain by NRA

GDOES analysis enabled us to obtain the evolution of the relative amount of nitrogen over the oxidation time. Ion beam analysis (IBA) was carried out to determine the nitrogen mass gain, using deuterons at 1.9 MeV as the incident beam and a TiN standard as the reference.

The nuclear reaction spectra show in the 1.4 – 10 MeV range different nuclear reactions of oxygen, nitrogen, and carbon (Fig. S6). They are given in Figure 6.a for oxidized samples and TiN standard in the 4 – 10 MeV range, where only nuclear reactions of ^{14}N are found. Among them, the $^{14}N(d,\alpha_1)^{12}C$ nuclear reaction was chose here to quantify nitrogen mass gain. This reaction has the dual advantage of having both a high effective cross-section, and a higher in-depth resolution than the $^{14}N(d,p_0)^{15}N$ reaction, thanks to higher energy losses for alpha particles than for protons of the same energy [27], [28]. For each nuclear reaction, the highest energy observed in the spectrum of the TiN standard corresponds to particles coming from the sample surface. For the $^{14}N(d,\alpha_1)^{12}C$ reaction, the maximum energy of α particles detected is 6788 keV. The lower the energy, the deeper the particles have been produced.

A zoomed view of the NRA spectra in the range of the $^{14}N(d,\alpha_1)^{12}C$ nuclear reaction is given in Figure 6.b. The energy spectra were used to calculate the depth distribution of the particles emitted, considering the stopping power of rutile. In addition, the intensity of NRA spectra compared to that of the TiN standard, taking into account the ratio of their respective stopping power, enables quantification of the nitrogen mass per unit volume. The results are given in

Figure 7 which shows the nitrogen concentration profile versus the depth for the samples oxidized for 15 min, 2 h, 16 h and 100 h. For the sample oxidized for 16 h, the depth of nitrogen insertion can be compared with the thickness of the oxidation layer in cross-section SEM views (Fig. 3.a,f,g), which varied from 300 nm to 1.3 µm in different areas. These values agree with the depth of nitrogen insertion shown in Fig. 7.

The nitrogen concentration profiles (Fig. 7) integrated over the depth provided the values of the nitrogen mass gain per surface area given in Table 1 together with their ratio over the total mass gain for the different oxidation durations. This ratio appears to be highest at the start of the oxidation process, decreasing after a few hours of exposure and stabilizing at around 2.5% after around 15 hours. The values obtained for the shortest oxidation durations should be treated with caution, however, given the very low mass of nitrogen inserted and the heterogeneities observed in the thickness of the oxide layer and in the location of the nitrogen (Fig.3.c). Despite this, the results suggest that nitrogen insertion is most rapid during a short transient exposure period of a few hours as also remarked in GDOES analysis (Fig. 4). A similar result was reported in a previous work [15] for CP-Ti oxidized at 700 °C. The ratio of nitrogen mass gain (also determined by NRA) to total mass gain decreased from 16% to 12% when the oxidation time was increased from 5 to 20 hours. Oxidation at a higher temperature leads in this case to a higher mass fraction of inserted nitrogen relative to the total mass gain, but as in the present study, the percentage of nitrogen in the mass gain decreases slightly with increasing oxidation duration.

The variation of the nitrogen mass gain (Table 1) is shown in Figure 8 as a function of the square root of the time of exposure, together with a linear fit according to the equation (1). As with the GDOES results (Fig. 5), the nitrogen mass gain for short oxidations lies slightly above the fitted line, but the overall experimental values fit well with linear variation up to 100 h. It

can be concluded that after a short transient period of a few hours, nitrogen insertion kinetics is parabolic up to 100 h, which agrees with the results of the GDOES analysis (Fig. 5).

The slope in the linear fit in Fig. 8 corresponds to a parabolic rate constant $k_p = 35 \times 10^{-7}$ $mg^2\,cm^{-4}\,h^{-1}$. This value is 1500 times smaller than the parabolic rate constant obtained for the total mass gain ($k_p = 53 \times 10^{-4}$ $mg^2\,cm^{-4}\,h^{-1}$). As nitrogen mass gain represents only a few percent of total mass gain, we can assume that oxygen mass gain kinetics is also parabolic as a function of exposure time, with nearly the same k_p value. Therefore, nitrogen insertion kinetics is around 1500 times slower than oxygen at 650 °C.

These results can be compared with those reported by Optasanu et al. [15] for CP-Ti oxidation at 700 °C in synthetic air for short exposure durations (5 and 20 h). Nitrogen mass gain was determined from NRA analyses as in the present article. From the nitrogen mass gain values at 5 and 20 h and assuming parabolic insertion kinetics, a k_p value of 90×10^{-7} $mg^2\,cm^{-4}\,h^{-1}$ can be estimated, slightly higher than that obtained here at 650 °C.

As shown in many previous works [8], [13], [14], [15], [22], the insertion mechanisms of oxygen and nitrogen into titanium at high temperatures are in competition. Under the conditions of this work, CP-Ti in air at 650°C, the oxidation is governed by an anionic diffusion mechanism through the oxide scale followed by diffusion through the metal. The presence of a nitride layer at the oxide/metal interface interferes with the diffusion of oxygen in the metal.

As regards diffusion of oxygen, the results obtained here show that the kinetics of the oxygen mass gain is parabolic, which corresponds to a diffusion driven process according to the classic Wagner theory of oxidation [21]. In the metal, the oxygen dissolves into the octahedral sites of titanium forming a solid solution. As far as nitrogen diffusion is concerned, the results obtained in this work show that nitrogen mass gain kinetics are also parabolic, but with a parabolic rate constant is 1500 times smaller compared to oxygen. The nitrogen occupies the same kind of

octahedral sites as oxygen when dissolved in titanium, which reduces the number of free sites free to be occupied by oxygen. However, the kinetics of nitrogen mass gain seems too slow compared to that of oxygen for this mechanism to explain the slower oxidation in air compared to pure oxygen. According to the literature, the nitrogen seems to diffuse faster than the oxygen in rutile [17] and almost two decades slower than oxygen in titanium [37], which leads to an progressive accumulation of nitrogen at the oxide/metal interface. The diffusion length of oxygen in titanium is much greater than that of nitrogen. In this work, the results of XRD and EDS-WDS analysis have shown the formation of an interfacial layer of tetragonal $Ti_2N_{0.84}$, which agrees with the observations reported in other works [13], [22]. The tetragonal structure of Ti_2N (rutile type structure) can be promoted by a possible epitaxial relationships with the tetragonal structure of rutile and the hcp structure of CP-Ti [38]. The formation of nitrides can also provide a mechanical accommodation layer between the oxide and the metal by decreasing the mechanical stress gradients.

The nitride interfacial layer acts as a barrier, slowing the diffusion of O^{2-} ions through the oxide. Optasanu et al. [15] have shown the nitrogen at the interface is continuously renewed due to the oxidation of nitrides by the flow of oxide ions. This leads to the formation of rutile, and releases nitrogen that can escape as a gas, probably promoting the formation of porosities, or diffuse inward over short distances into the metal to form new $Ti_2N_{0.84}$. Nitrogen remains consequently at the oxide/metal interface, which is progressively shifted inward. Nitride oxidation requires a certain amount of activation energy, allowing Ti-N bonds to be broken and Ti-O bonds to be formed. This induces an increase in oxygen partial pressure at the nitride-oxide interface, resulting in a decrease in oxygen flow through the oxide layer to the oxide/nitride interface, and consequently slowing down the oxidation rate.

All this suggests that the flow of oxygen through the oxide layer governs the kinetics of the nitrogen remaining at the interface, but at the same time the interfacial nitride oxidation reaction induces a decrease of the flow of oxygen which slows down the oxidation.

4. Conclusions

This work investigated the insertion of nitrogen into commercially pure titanium oxidized at 650 °C in air from the early stages of oxidation up to 100 h. The main objectives were to quantify the nitrogen mass gain and determine its kinetics.

The insertion of nitrogen from the earliest stage of oxidation (15 min) and its location at the oxide-metal interface were shown by NRA and GDOES analysis. Cross-sectional SEM observations of samples oxidized for 16 h confirm the localization of nitrogen at the oxide-metal interface, in agreement with previous works.

The following conclusions can be drawn from this study:

- In the early stages of oxidation, 15 minutes, nitrogen mass gain is estimated from NRA results at 2.3×10^{-3} mg cm^{-2}, and it increases up to 18.7×10^{-3} mg cm^{-2} for an exposure time of 100 h.
- Below 2h of exposure, the ratio of nitrogen mass to total mass gain can be roughly estimated at around 6-9%. After 2h of exposure and up to 100 h, this ratio decreases and stabilizes at around 2.5%.
- After a short transient period, the kinetics of nitrogen mass gain is parabolic up to 100 h.

- The parabolic rate constant for the nitrogen mass gain, $k_p = 35 \times 10^{-7}$ mg^2 cm^{-4} h^{-1}, is about 1500 times smaller than the parabolic rate constant obtained for the total mass gain $k_p = 53 \times 10^{-4}$ mg^2 cm^{-4} h^{-1}.
- Assuming that oxygen insertion follows a parabolic kinetics analogous to the total mass gain, largely due to oxygen mass gain, one can conclude that nitrogen inserts into CP-Ti about 1500 times more slowly than oxygen at 650 °C in air.

Finally, a description of the oxidation process of CP-Ti in air has been proposed, in which the nitride layer formed at the oxide-metal interface is the key factor in slowing the oxidation rate of titanium.

The results underline the value of using ion beam analysis techniques such as NRA to study the role of nitrogen in the high-temperature oxidation of titanium alloys in air.

Acknowledgments

This work was supported by the EIPHI Graduate School (contract ANR-17-EURE-0002). V. B. acknowledges support from the French Ministry of National Education, Higher Education and Research, MENRT fellowship.

Data availability

The raw/processed data required to reproduce these findings cannot be shared at this time as the data also forms part of an ongoing study.

References

[1] M. Peters, J. Kumpfert, C. H. Ward, et C. Leyens, « Titanium Alloys for Aerospace Applications », *Adv. Eng. Mater.*, vol. 5, nº 6, p. 419-427, juin 2003, doi: 10.1002/adem.200310095.

[2] I. Inagaki, Y. Shirai, T. Takechi, et N. Ariyasu, « Application and Features of Titanium for the Aerospace Industry », nº 106, 2014.

[3] P. Singh, H. Pungotra, et N. S. Kalsi, « On the characteristics of titanium alloys for the aircraft applications », *Int. Conf. Adv. Aeromechanical Mater. Manuf. ICAAMM-2016 Organ. MLR Inst. Technol. Hyderabad Telangana India*, vol. 4, nº 8, p. 8971-8982, janv. 2017, doi: 10.1016/j.matpr.2017.07.249.

[4] J. Halchak, « Spacecraft Materials », in *Encyclopedia of Materials: Science and Technology*, K. H. J. Buschow, R. W. Cahn, M. C. Flemings, B. Ilschner, E. J. Kramer, S. Mahajan, et P. Veyssière, Éd., Oxford: Elsevier, 2001, p. 8755-8758. doi: https://doi.org/10.1016/B0-08-043152-6/01567-9.

[5] K. S. Chan, M. Koike, B. W. Johnson, et T. Okabe, « Modeling of Alpha-Case Formation and Its Effects on the Mechanical Properties of Titanium Alloy Castings », *Metall. Mater. Trans. A*, vol. 39, nº 1, p. 171-180, janv. 2008, doi: 10.1007/s11661-007-9406-0.

[6] T. Wang, B. Li, Z. Wang, et Z. Nie, « A microstructure with improved thermal stability and creep resistance in a novel near-alpha titanium alloy », *Mater. Sci. Eng. A*, vol. 731, p. 12-20, juill. 2018, doi: 10.1016/j.msea.2018.06.034.

[7] X. Zhong *et al.*, « Improving thermal stability and creep resistance by Sc addition in near-α high-temperature titanium alloy », *J. Mater. Sci. Technol.*, vol. 183, p. 1-11, juin 2024, doi: 10.1016/j.jmst.2023.09.056.

[8] A. M. Chaze et C. Coddet, « The role of nitrogen in the oxidation behaviour of titanium and some binary alloys », *J. Common Met.*, vol. 124, nº 1-2, p. 73-84, oct. 1986, doi: 10.1016/0022-5088(86)90478-9.

[9] A. M. Chaze et C. Coddet, « Influence of alloying elements on the dissolution of oxygen in the metallic phase during the oxidation of titanium alloys », *J. Mater. Sci.*, vol. 22, p. 1206-1214, 1987.

[10] A. Kanjer *et al.*, « Effect of laser shock peening on the high temperature oxidation resistance of titanium », *Surf. Coat. Technol.*, vol. 326, p. 146-155, oct. 2017, doi: 10.1016/j.surfcoat.2017.07.042.

[11] A. Kanjer *et al.*, « Influence of Mechanical Surface Treatment on High-Temperature Oxidation of Pure Titanium », *Oxid. Met.*, vol. 88, nº 3-4, p. 383-395, oct. 2017, doi: 10.1007/s11085-016-9700-6.

[12] C. Dupressoire, A. Rouaix-Vande Put, P. Emile, C. Archambeau-Mirguet, R. Peraldi, et D. Monceau, « Effect of Nitrogen on the Kinetics of Oxide Scale Growth and of Oxygen Dissolution in the Ti6242S Titanium-Based Alloy », *Oxid. Met.*, vol. 87, nº 3, p. 343-353, avr. 2017, doi: 10.1007/s11085-017-9729-1.

[13] I. Abdallah, C. Dupressoire, L. Laffont, D. Monceau, et A. Vande Put, « STEM-EELS identification of TiOXNY, TiN, Ti2N and O, N dissolution in the Ti2642S alloy oxidized in synthetic air at 650 °C », *Corros. Sci.*, vol. 153, p. 191-199, juin 2019, doi: 10.1016/j.corsci.2019.03.037.

[14] C. Dupressoire *et al.*, « The role of nitrogen in the oxidation behaviour of a Ti6242S alloy: a nanoscale investigation by atom probe tomography », *Acta Mater.*, vol. 216, p. 117134, sept. 2021, doi: 10.1016/j.actamat.2021.117134.

[15] V. Optasanu *et al.*, « Nitrogen quantification and tracking during high temperature oxidation in air of titanium using 15N isotopic labelling », *Corros. Sci.*, vol. 216, p. 111072, mai 2023, doi: 10.1016/j.corsci.2023.111072.

[16] L. Lavisse *et al.*, « Tracking the role of nitrogen in the improvement of the high temperature oxidation resistance of titanium by mechanical treatments », *Corros. Sci.*, vol. 197, p. 110080, avr. 2022, doi: 10.1016/j.corsci.2021.110080.

[17] M. Raffy, « Thèse de doctorat ». Éc. Natl. Supér. de Chim. de Paris, 1981.

[18] A. Anttila, J. Räisänen, et J. Keinonen, « Diffusion of nitrogen in α-Ti », *Appl. Phys. Lett.*, vol. 42, nº 6, p. 498-500, mars 1983, doi: 10.1063/1.93981.

[19] D. David, G. Beranger, et E. A. Garcia, « A Study of the Diffusion of Oxygen in α-Titanium Oxidized in the Temperature Range 460°–700°C », *J. Electrochem. Soc.*, vol. 130, nº 6, p. 1423-1426, juin 1983, doi: 10.1149/1.2119966.

[20] Z. Liu et G. Welsch, « Literature Survey on Diffusivities of Oxygen, Aluminum, and Vanadium in Alpha Titanium, Beta Titanium, and in Rutile », *Metall. Trans. A*, vol. 19, nº 4, p. 1121-1125, avr. 1988, doi: 10.1007/BF02628396.

[21] P. Kofstad, *High Temperature Corrosion*, Elsevier Applied Science. 1988.

[22] M. R. Aldaz Cervantes, « Fundamentals of Titanium Interactions with Nitrogen and Oxygen », UC Santa Barbara, 2022. [En ligne]. Disponible sur: ProQuest ID: AldazCervantes_ucsb_0035D_15613. Merritt ID: ark:/13030/m5t79th9. Retrieved from https://escholarship.org/uc/item/24j1b2cr

[23] M. Göbel, J. D. Sunderkötter, D. I. Mircea, H. Jenett, et M. F. Stroosnijder, « Study of the high-temperature oxidation behaviour of Ti and Ti4Nb with SNMS using tracers », *Surf. Interface Anal.*, vol. 29, nº 5, p. 321-324, mai 2000, doi: 10.1002/(SICI)1096-9918(200005)29:5<321::AID-SIA872>3.0.CO;2-Q.

[24] T. C. Valenza, P. Chao, P. K. Weber, O. K. Neill, et E. A. Marquis, « Protective role of silicon in the high-temperature oxidation of titanium », *Corros. Sci.*, vol. 217, p. 111110, juin 2023, doi: 10.1016/j.corsci.2023.111110.
[25] T. C. Valenza, P. K. Weber, et E. A. Marquis, « Role of niobium in the high-temperature oxidation of titanium », *Corros. Sci.*, vol. 225, p. 111603, déc. 2023, doi: 10.1016/j.corsci.2023.111603.
[26] C. Dupressoire *et al.*, « The role of nitrogen in the oxidation behaviour of a Ti6242S alloy: a nanoscale investigation by atom probe tomography », *Acta Mater.*, vol. 216, p. 117134, sept. 2021, doi: 10.1016/j.actamat.2021.117134.
[27] P. Trocellier, P. Berger, et M. Wilde, « Nuclear Reaction Analysis », *Encycl. Anal. Chem.*, p. 1-17, 2016, doi: 10.1002/9780470027318.a6208.pub3.
[28] M. Peisach, « Nuclear Reaction Analysis », *Elem. Anal. Part. Accel.*, 1992.
[29] Agence internationale de l'énergie atomique, « Ion beam techniques for the analysis of light elements in thin films, including depth profiling: final report of a co-ordinated research project 2000-2003 », *Vienna: International Atomic Energy Agency*, [online], 2004. Consulté le: 30 novembre 2021. [En ligne]. Disponible sur: http://www-pub.iaea.org/MTCD/publications/PDF/te_1409_web.pdf
[30] H. Khodja, E. Berthoumieux, L. Daudin, et J.-P. Gallien, « The Pierre Süe Laboratory nuclear microprobe as a multi-disciplinary analysis tool », *Nucl. Instrum. Methods Phys. Res. Sect. B Beam Interact. Mater. At.*, vol. 181, nº 1-4, p. 83-86, juill. 2001, doi: 10.1016/S0168-583X(01)00564-X.
[31] P. Berger et G. Revel, « Microsonde nucléaire - Principe et appareillage », *Tech. Ing.*, vol. TIB389DUO, p. 19, sept. 2005, doi: 10.51257/a-v3-p2563.
[32] P. Trouslard, J. Frontier, « Pyrole: a user friendly software for teaching IBA and analysing experimental data, INIS mf-14707. »
[33] T. Kitashima, T. Hara, Y. Yang, et Y. Hara, « Oxidation–nitridation-induced recrystallization in a near-α titanium alloy », *Mater. Des.*, vol. 137, p. 355-360, janv. 2018, doi: 10.1016/j.matdes.2017.10.043.
[34] R. Escobar Galindo, R. Gago, J. M. Albella, R. Escobar Galindo, R. Gago, et A. Lousa, « Comparative depth-profiling analysis of nanometer-metal multilayers by ion-probing techniques », *TrAC Trends Anal. Chem.*, vol. 28, nº 4, p. 494-505, avr. 2009, doi: 10.1016/j.trac.2009.01.004.
[35] Y. Liu, W. H. Yu, et J. Y. Wang, « A model for quantification of GDOES depth profiles », *Vacuum*, vol. 113, p. 5-10, mars 2015, doi: 10.1016/j.vacuum.2014.11.015.
[36] M. Wilke *et al.*, « Glow discharge optical emission spectroscopy for accurate and well resolved analysis of coatings and thin films », *Thin Solid Films*, vol. 520, nº 5, p. 1660-1667, déc. 2011, doi: 10.1016/j.tsf.2011.07.058.
[37] H. Nakajima et M. Koiwa, « Diffusion in Titanium », *ISIJ Int.*, vol. 31, nº 8, p. 757-766, 1991, doi: 10.2355/isijinternational.31.757.
[38] E. Lenarduzzi, P. Bounie, C. Schuman, M. -J. Philippe, et D. Petelot, « Titanium Oxidation During Thermal Treatment: Inhibiting Role of Nitrogen and Epitaxial Orientation Relations Evidenced by EBSD », *Adv. Eng. Mater.*, vol. 5, nº 8, p. 587-593, août 2003, doi: 10.1002/adem.200300390.

FIGURE CAPTIONS

Figure 1 - CP-Ti mass gain (mg cm^{-2}) as a function of square root of time at 650 °C in air for small samples in black circle (samples used for NRA), and large samples in red square (samples used for GDOES).

Figure 2 - Grazing incidence XRD patterns obtained for CP-Ti before oxidation and after 16 and 80 h at 650 °C in air. The incidence angle was 8°.

Figure 3 - SEM cross-section images of CP-Ti oxidized in air at 650°C for 16 hours: (a) BSE image, (b,c,d) element distribution in the same area: (b) EDS mapping of oxygen, (c) WDS mapping of nitrogen (d) EDS mapping of titanium, (e) enlarged view of part of image (a) with enhanced contrast, (f) and (g) high-magnification images of the oxidation layer in the thin and thick areas, respectively.

Figure 4 - (a) GDOES profiles of oxygen, nitrogen, and titanium over sputtering time for the sample oxidized for 15 minutes, and (b) GDOES profiles of nitrogen over the sputtering time for samples oxidized for 15 min, 2 h, 16 h and 100 h. The multiplicative factors, O(x3) and Ti(/200), are only used to ensure a good visibility of the profiles.

Figure 5 - Variation in the relative amount of nitrogen calculated by integrating the profiles obtained by GDOES, as a function of the square root of the oxidation time.

Figure 6 - (a) Nuclear reaction spectra of CP-Ti samples oxidized for 15 min (in green), 2 h (in orange), 16 h (in red) and 100 h (in black), and of a pure TiN standard (intensity divided by 4). Incident beam: deuterons with an energy of 1.9 MeV. Detection at 170°, annular detector. (b) Enlarged view of Figure 6.a in the range of the $^{14}N(d,\alpha_1)^{12}C$ nuclear reaction.

Figure 7 - Evolution of nitrogen concentration (mg cm^{-3}) over depth from the surface of the sample, calculated from NRA profiles, for CP-Ti samples oxidized in air at 650°C from 15 min to 100 h.

Figure 8 - Nitrogen mass gain (mg cm^{-2}), calculated from nitrogen NRA profiles, over the square root of the oxidation time in air at 650°C.

Highlights

- Nitrogen insertion in CP-Ti oxidized at 650°C in air was studied up to 100 h
- Nuclear Reaction Analysis provided nitrogen depth profiles and mass gain
- 2.5% of the total mass gain corresponds to nitrogen in 100h-oxidized samples
- The kinetics of nitrogen mass gain as a function of time is parabolic up to 100 h
- Oxygen insertion is also parabolic with time, but 1500 times faster than nitrogen

Figure1

Click here to access/download;Figure;

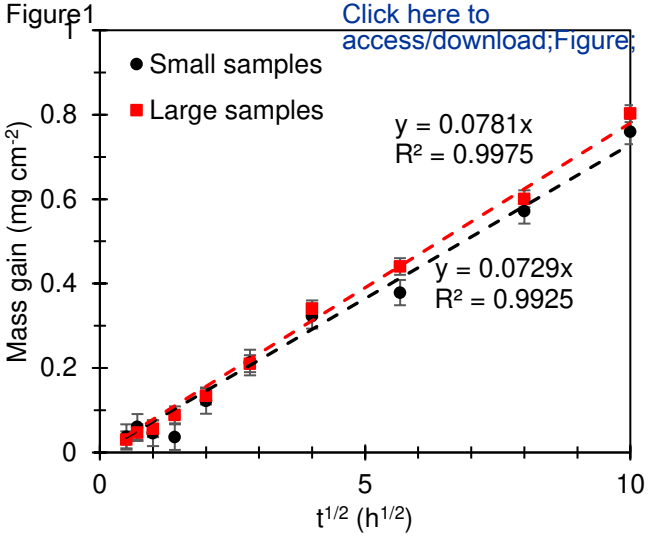

Figure2

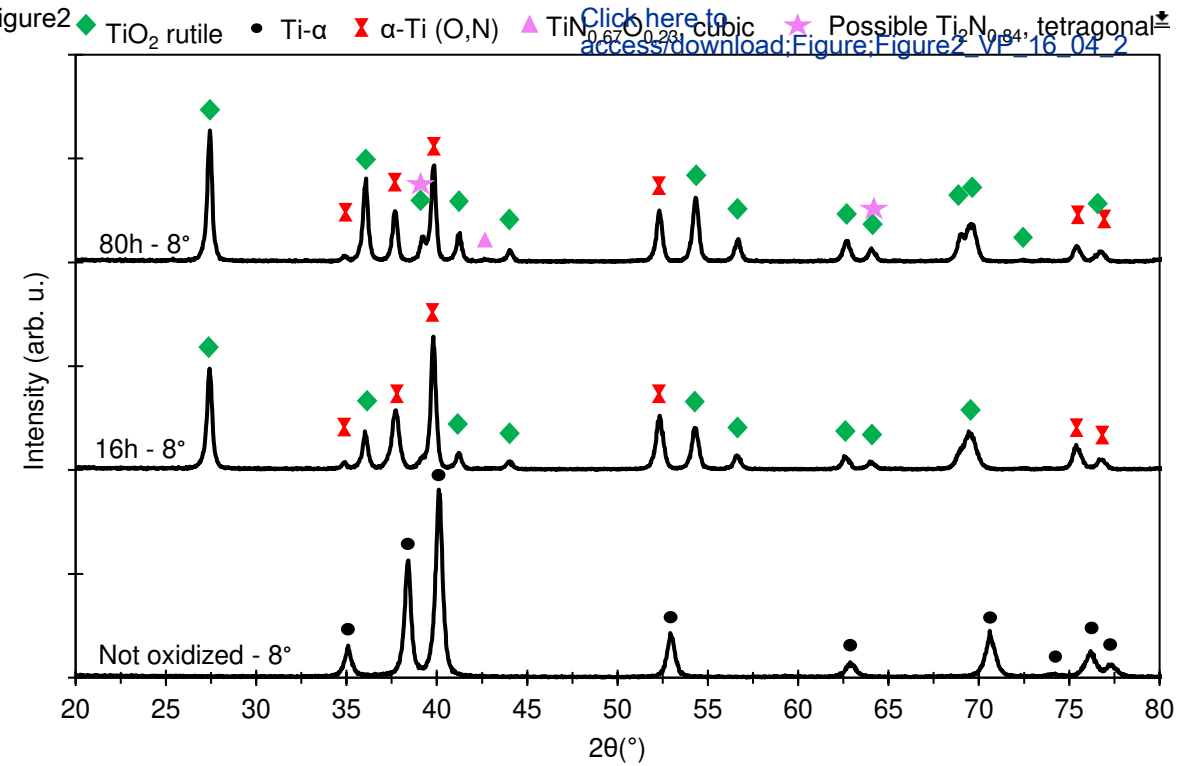
Click here to access/download;Figure;Figure2_VP_16_04_2
TiO2 rutile
Ti-α
α-Ti (O,N)
TiN0.67O0.28, cubic
Possible Ti2N0.84, tetragonal
80h - 8°
16h - 8°
Not oxidized - 8°
Intensity (arb. u.)
20
25
30
35
40
45
50
55
60
65
70
75
80
2θ(°)

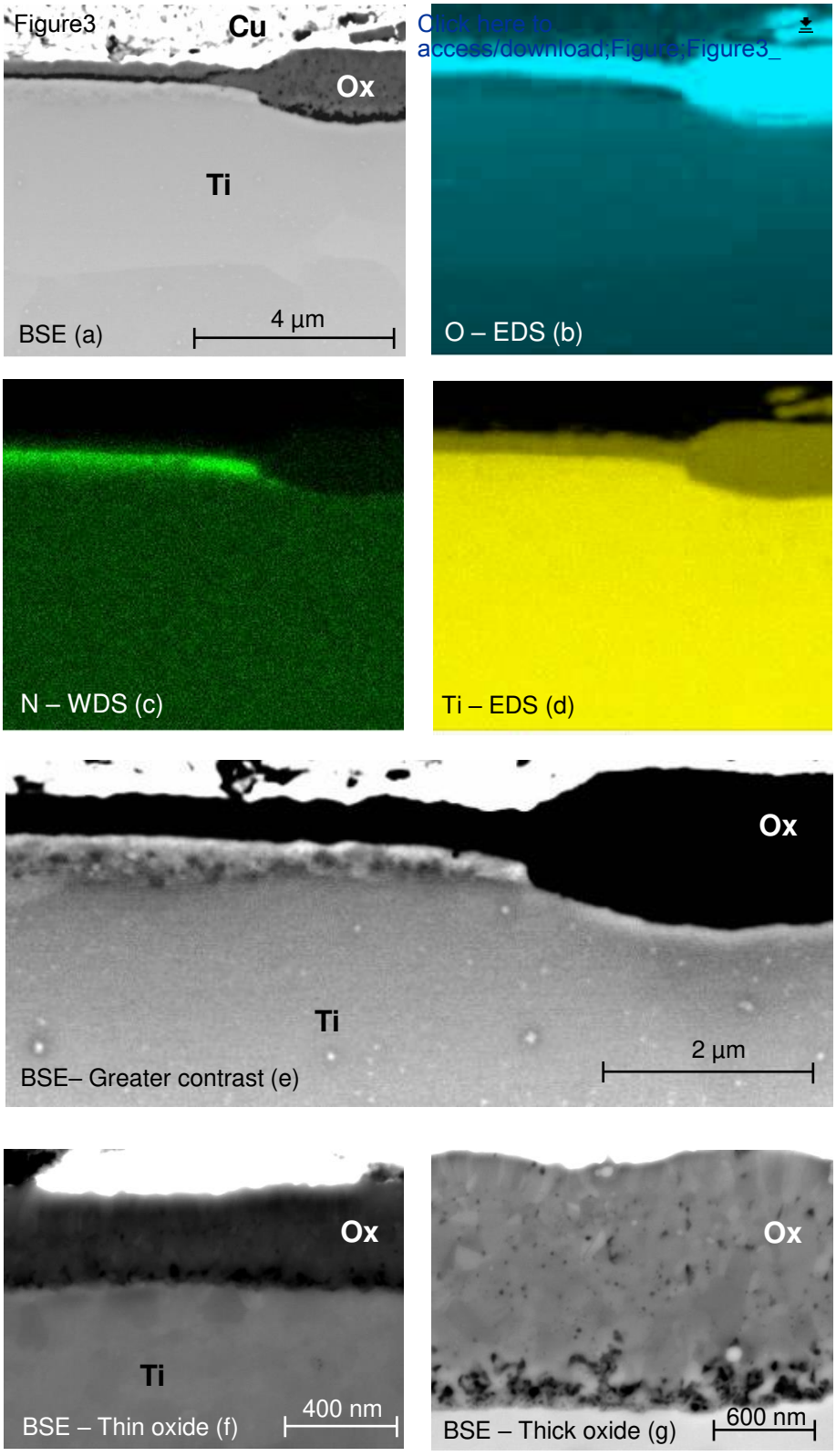
Figure3
Cu
Ox
Ti
BSE (a)
4 µm
Click here to access/download;Figure;Figure3_
O – EDS (b)
N – WDS (c)
Ti – EDS (d)
Ox
Ti
BSE– Greater contrast (e)
2 µm
Ox
Ti
BSE – Thin oxide (f)
400 nm
Ox
BSE – Thick oxide (g)
600 nm

Figure4

Click here to access/download;Figure;Figure4_V

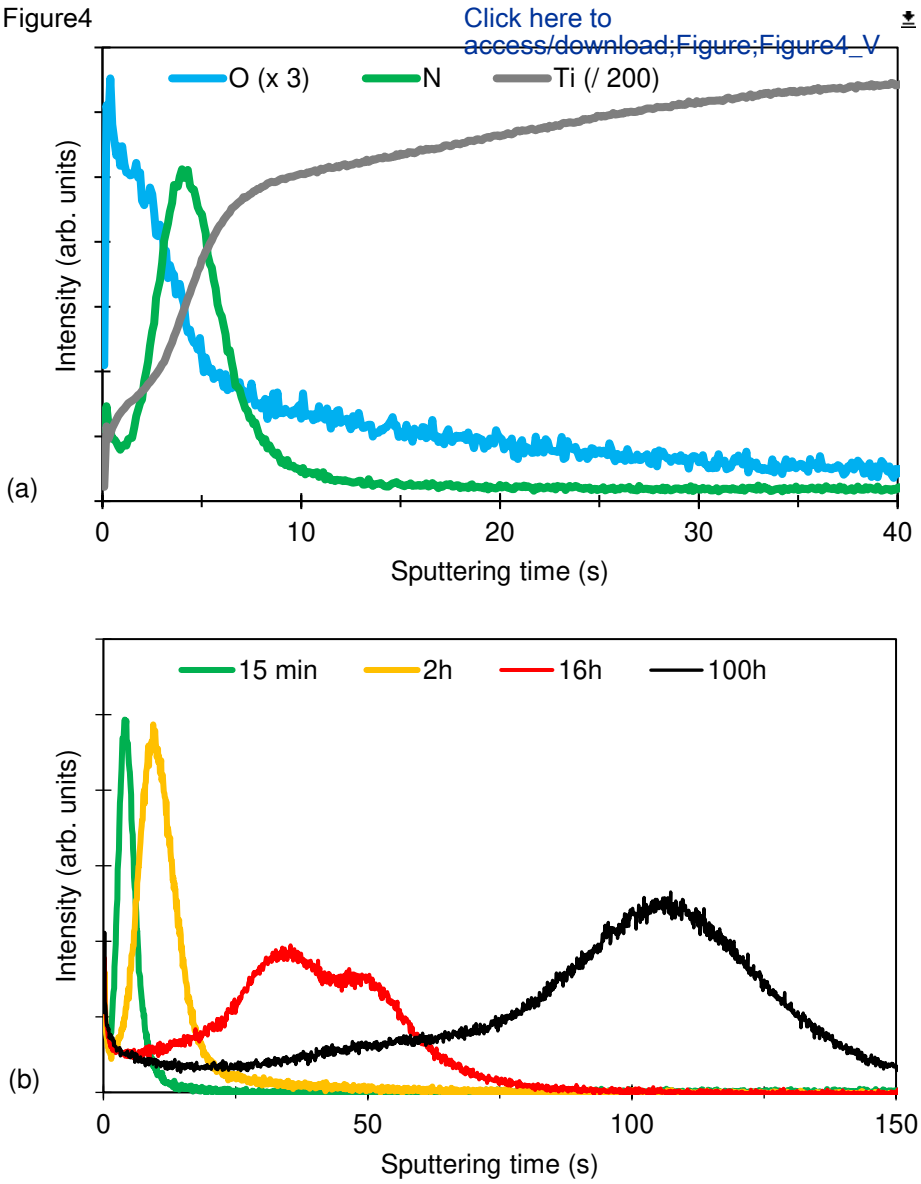

Figure 5

Click here to access/download;Figure;Fig

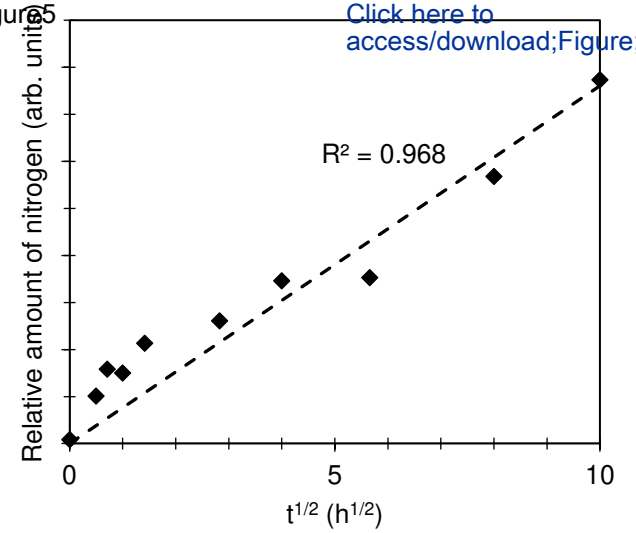

Figure6

Click here to access/download;Figure;Figure6_VP

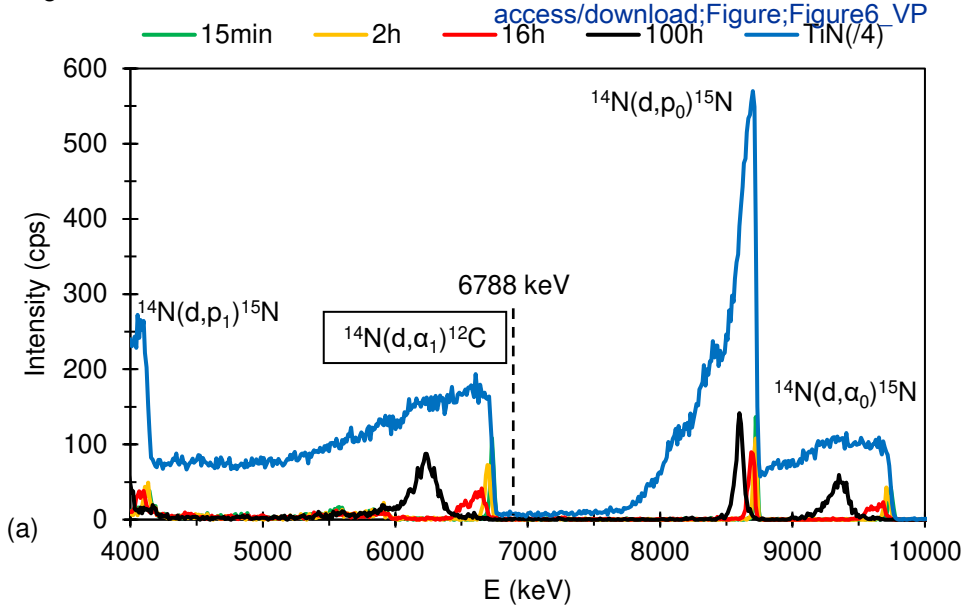

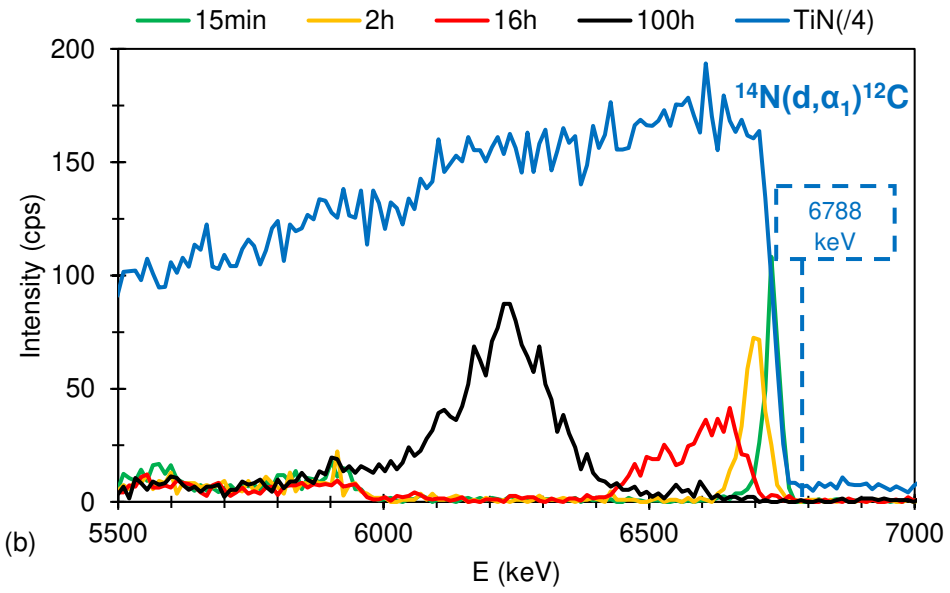

Figure7

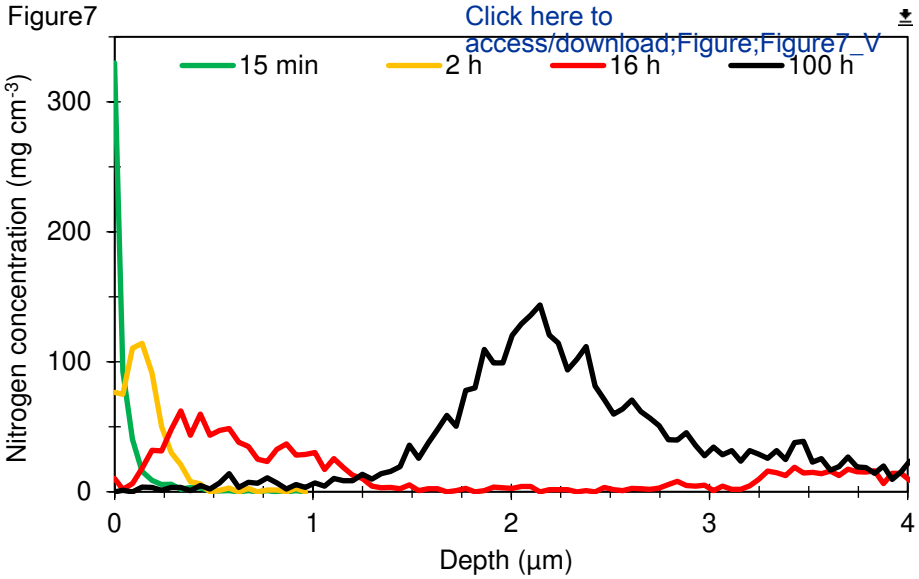

Figure8

Click here to access/download;Figure;F

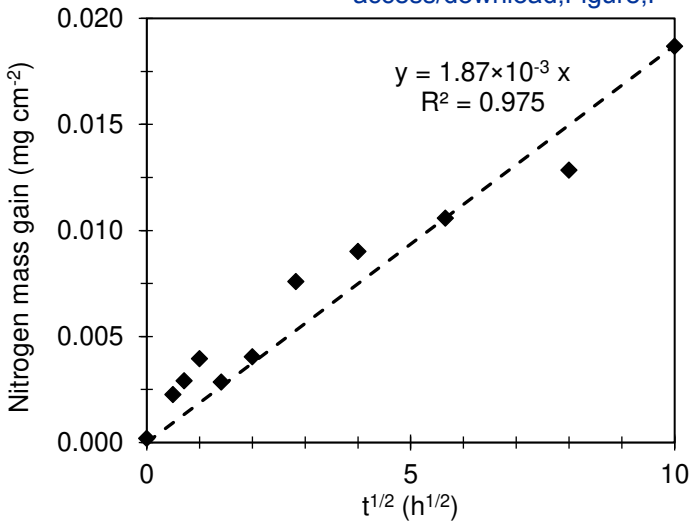

TABLES

Table 1. Nitrogen mass gain, calculated from nitrogen NRA profiles, and its ratio over total mass gain for different oxidation times for CP-Ti at 650 °C in air.

Table 1

Oxidation time (h)	Nitrogen mass gain (10^{-3} mg cm^{-2})	Nitrogen mass gain vs. total mass gain (%)
0.25	2.3	6.1
0.5	2.9	4.8
1	4.0	8.7
2	2.8	7.8
4	4.1	3.3
8	7.6	3.6
16	9.0	2.8
32	10.6	2.8
64	12.8	2.2
100	18.7	2.5

Supplementary Information

Quantification and kinetics of nitrogen mass gain during high temperature oxidation of titanium in air

Victor Pacorel[1], Pascal Berger[2], Virginie Moutarlier[3], María del Carmen Marco de Lucas[1], Tony Montesin[1], Nicolas Geoffroy[1], Frédéric Herbst[1], Olivier Heintz[1], Virgil Optasanu[1], Luc Lavisse[1,*]

[1]Laboratoire Interdisciplinaire Carnot de Bourgogne (ICB), UMR 6303 CNRS-Université de Bourgogne, 9 Avenue A. Savary, BP 47 870, F-21078, Dijon, France

[2] Université Paris-Saclay, CEA, CNRS, NIMBE, 91191, Gif-sur-Yvette, France

[3] Institut UTINAM, UMR CNRS 6213, 16 Route de Gray, Université Franche-Comté, 25030, Besançon, France

1. Structure and phases of the oxidized samples

1.1 X-Ray diffraction

Grazing incidence X-ray diffraction was used to identify the crystalline phases present in the oxidized samples. The incidence angle was θ_{inc} = 8°.

Figure S1 shows a zoomed view of grazing incidence XRD patterns obtained for Ti-CP after 16 and 80 h at 650 °C in air, in the regions where diffraction reflections of titanium nitride phases can be expected. After 80 h of oxidation, new peaks can also be distinguished in the XRD pattern at around 39,2°, 42,6° and 69,0°. Two of these, at 39.2° and 69.0°, correspond to the positions of XRD peaks reported for tetragonal titanium nitride $Ti_2N_{0.83}$ (ICDD 04-002-0574), while the very weak peak at 42.6° corresponds to the position of an XRD peak of titanium oxynitride $TiN_{0.67}O_{0.23}$ (ICDD 04-006-2333).

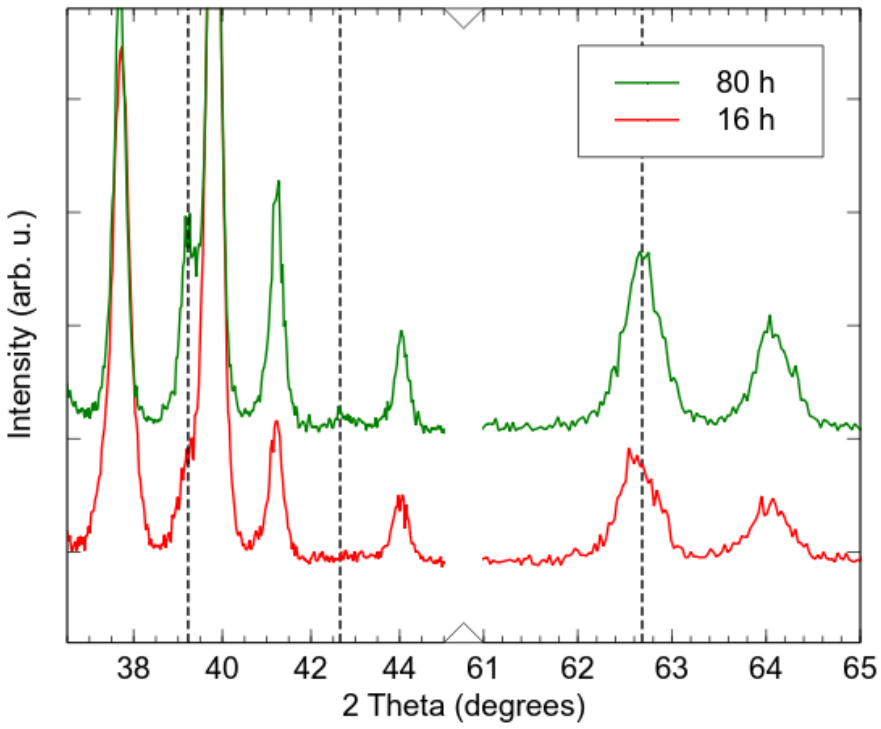

Figure S1. Zoomed view of grazing incidence XRD patterns obtained for CP-Ti after 16 and 80 h at 650 °C in air. The incidence angle was 8°.

1.2 SEM cross-section images

Figure S2.a shows a low-magnification SEM cross-section image in BSE mode of a sample oxidized for 16 hours at 650°C in air. From bottom to top of the image, one can see the Ti metal substrate, the oxidation layer, the sputtered gold layer and the thick layer of electrodeposited copper. Figure S2.b shows a high-magnification SEM cross-section image in BSE mode of the same sample oxidized for 16 hours at 650°C in air.

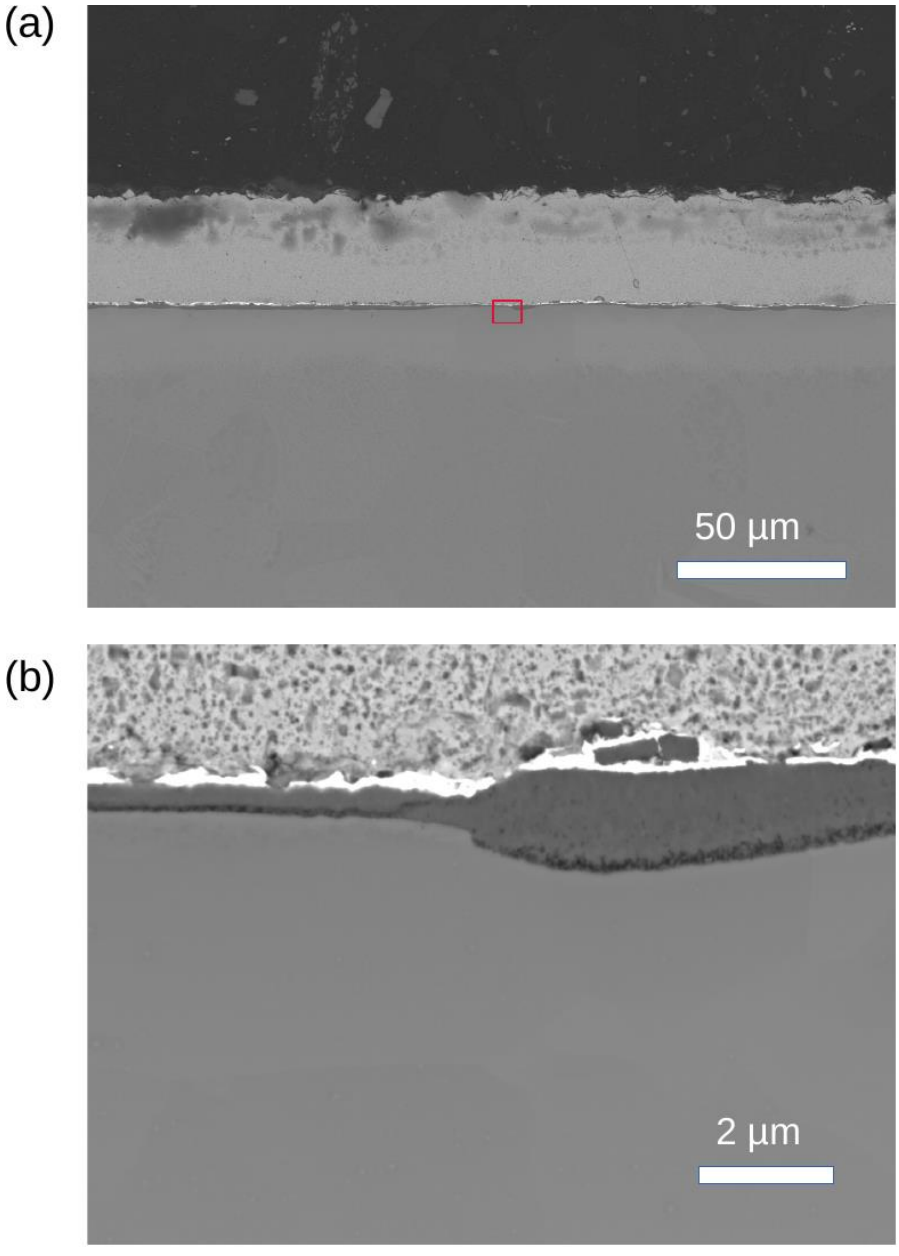

Figure S2. (a) Low-magnification, and (b) high magnification cross-section images in BSE mode of CP-Ti oxidized in air at 650 °C for 16 hours. The area corresponding to the SEM images given in Figure 3 is shown in red.

2. Elemental composition profiles by GDOES

Glow-Discharge Optical Emission Spectroscopy was used to study the in-depth elemental composition. The spectrometer was a Jobin-Yvon Horiba GD Profiler (U = 600V), calibrated on aluminium ray with a pure aluminium plate. The size of the zone analysed was 4 mm in diameter. The distribution of oxygen, nitrogen and titanium was monitored by measuring the evolution over sputtering time of the intensity of the radiation characterizing each element: 130.21 nm, 149.26 nm, and 365.35 nm, respectively.

GDOES profiles of titanium, nitrogen, and nitrogen over the erosion time obtained for the samples oxidized 15 min, 2 h, 16 h and 100 h are shown in Figures S3 (nitrogen and titanium) and S4 (oxygen and titanium).

GDOES oxygen profiles were integrated over the duration of erosion for the different oxidation times. Figure S5 shows the obtained values, normalized to that of the sample oxidized for 100 h, as function of the square root of the oxidation time. It provides the evolution of the relative concentration of oxygen.

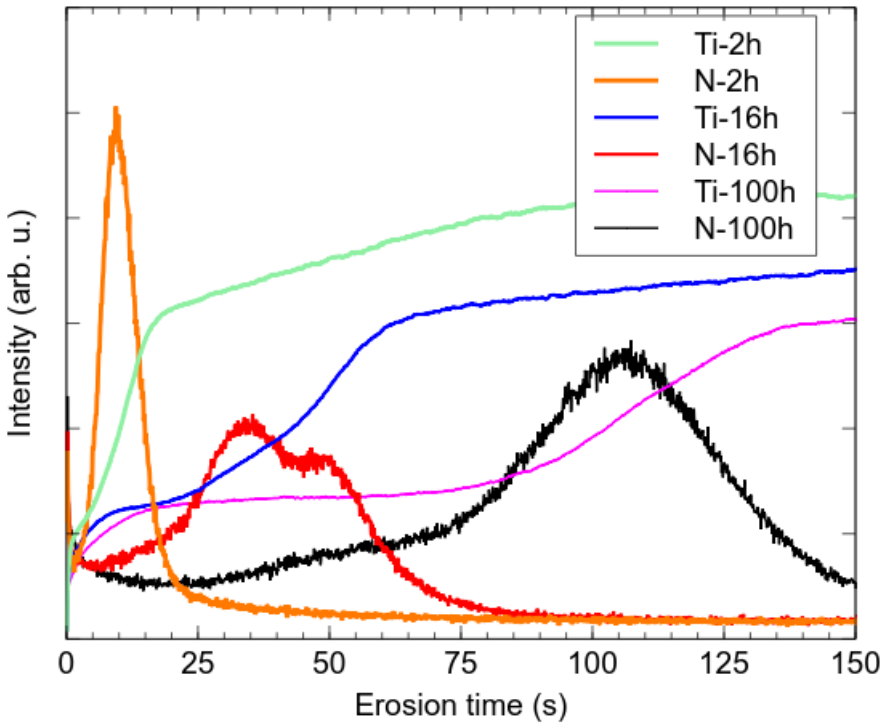

Figure S3. GDOES profiles of titanium and nitrogen over the erosion time for the samples oxidized 15 min, 2 h, 16 h and 100 h.

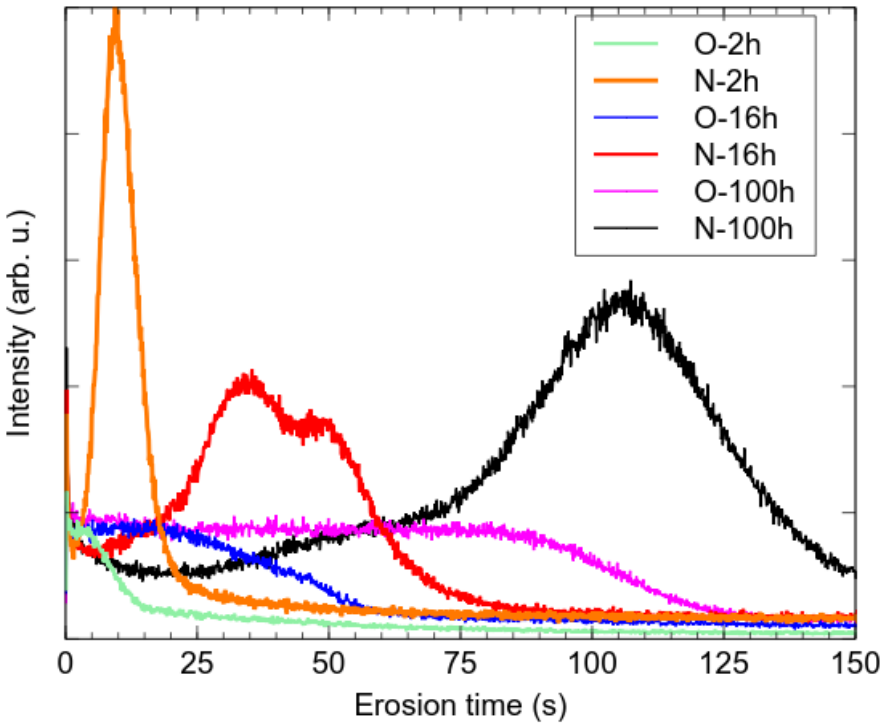

Figure S4. GDOES profiles of oxygen and nitrogen over the erosion time for the samples oxidized 15 min, 2 h, 16 h and 100 h.

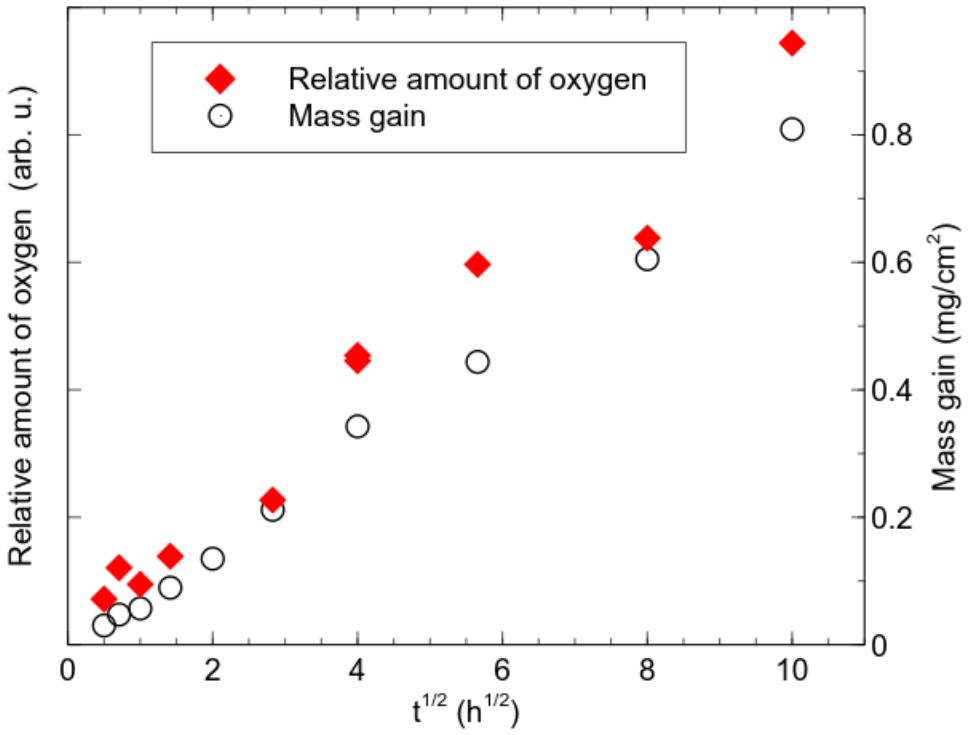

Figure S5. Total mass gain and relative amount of oxygen, calculated from GDOES profiles of oxygen, as a function of the square of the oxidation time.

3. Quantifying nitrogen mass gain by NRA

Ion beam analysis was carried out using deuterons at 1.9 MeV as the incident beam and a TiN standard as the reference. The detection of backscattered deuterons and particles produced by the nuclear reactions was done at 170° from the incident deuteron beam using an annular barrier detector.

Figure S6 shows nuclear reaction spectra of CP-Ti samples oxidized for 15 min (in green), 2 h (in orange), 16 h (in red) and 100 h (in black), and of a pure TiN standard (intensity reduced by 4).

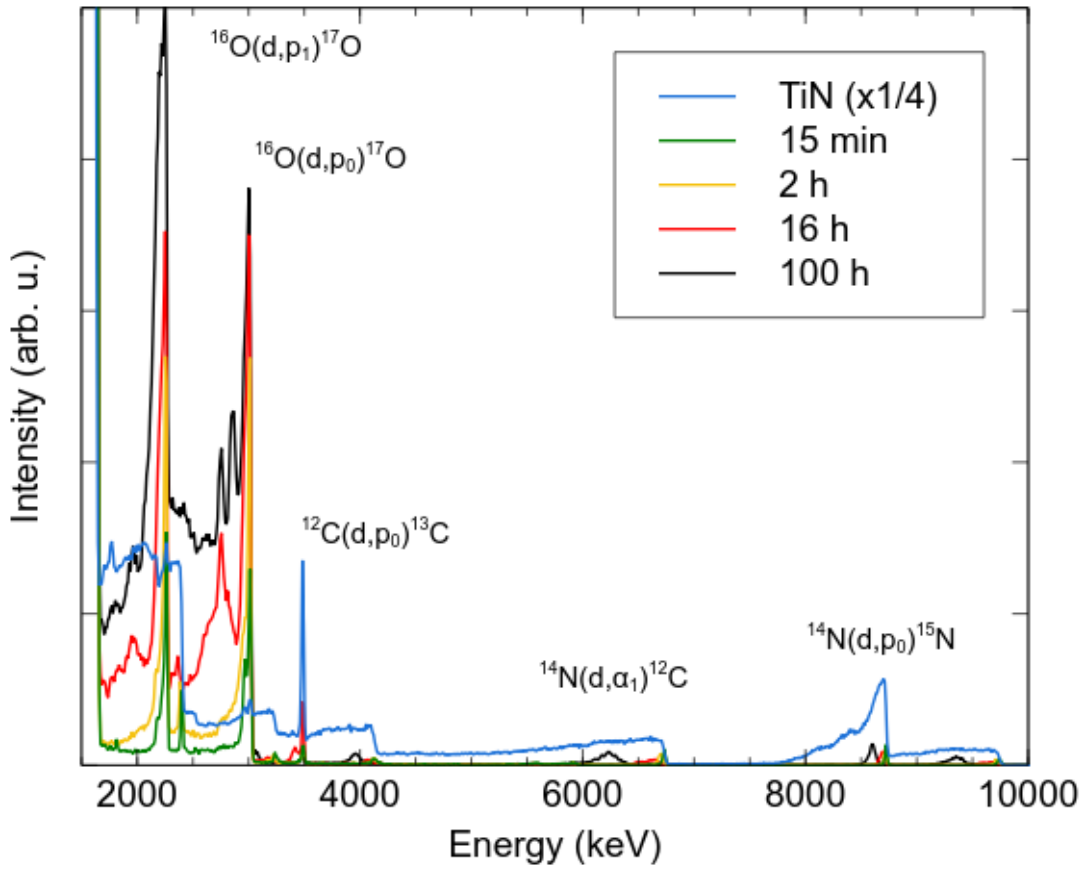

Figure S6. Nuclear reaction spectra of CP-Ti samples oxidized for 15 min (in green), 2 h (in orange), 16 h (in red) and 100 h (in black), and of a pure TiN standard (intensity divided by 4). Incident beam: deuterons with an energy of 1.9 MeV. Detection at 170° in front of the annular detector.